Building and Environment 196 (2021) 107807

Contents lists available at ScienceDirect

Building and Environment

journal homepage: http://www.elsevier.com/locate/buildenv

Renovation and innovation using thermal insulation lining systems - Acoustic performance

C. Churchill [a,*], T. Bednar [a], H. Müllner [b], M. Neusser [c], S. Hinterseer [a]

[a] TU Wien, Karlsplatz 13/207-02, A-1040, Wien, Austria
[b] TGM, Wexstraße 19-23, 1200, Wien, Austria
[c] ACOM Research, Kienegg 27, 2813, Thomasberg, Austria

A B S T R A C T

Retrofit and design of thermal cladding systems provide an opportunity to improve the acoustic properties of a building. However, the complexity of the calculation process to predict sound insulation improvement may inhibit rather than encourage novelty and innovation. This paper investigates whether it is realistic to calculate the frequency dependant sound insulation improvement due to modern thermal insulation wall lining systems with just a few input parameters. The calculation procedure is tested using measured results for one external thermal insulation composite system (ETICS) and three curtain wall systems. The accuracy of the procedure is examined using three factors: (1) precision of the measurement, (2) variation of some of the basic parameters of the calculation procedure, and (3) an estimation of the standard error of the calculation. For the ETICS, agreement within <6.0 dB is achieved across much of the frequency range and the trend of the extended dip due to the spring-mass action of the panel is corroborated. The case for using this methodology on curtain wall systems is adequate, however, the trend of calculated results is mostly outside of the 95% confidence limits of the measured results. Possible reasons for this include lack of airtightness of all curtain wall systems and additional transmission due to radiation into and out of the cavity, neither of which are included in the model. The assumption of radiating points or lines, rather than a radiating surface involving the whole panel, gave better agreement at high frequencies for three of the four measured systems ($f \geq 2500$ Hz).

1. Introduction

Improving the cladding of a building can reduce the quantity of energy consumed during the operational phase [1], and examples of thermal insulation lining systems in retrofit [2–6] and construction [7–11] can be found worldwide; particularly where climates reach sub-zero temperatures. However, the thermal retrofit of buildings may result in an acoustic disadvantage, for example, when a resonance frequency falls within the building acoustics range (50 Hz–5000 Hz). It would instead be preferable that the retrofit is deemed an opportunity to improve the acoustic properties of the building [12], termed the "free dB concept" [2]. However, the lack of standardised tools to assess the acoustic impact of a layer across the building acoustics frequency range does not align with the market incentive for building specialists to develop acoustically optimised linings. There is also underlying concern that analytical-based prediction models can be cumbersome to implement and may be overly complicated for the problem at hand. A review of regulations and standards should address these concerns.

There are three broad and overlapping categories of prediction model capable of predicting the sound insulation improvement (ΔR) of cladding systems. These are: (1) transfer matrix method (TMM) (2) statistical energy analysis (SEA) approach, and (3) other methodologies such as wave-based or semi-empirical approaches. The TMM arose from the earlier progressive impedance method (PIM) [13] established to determine the sound insulation through alternating layers of materials, such as flexible blankets, metal sheets and air spaces in aircraft and other similar applications [14]. When many layers are involved the PIM can become a laborious effort to progressively sum the physical effects through the layers. Instead the TMM enables a matrix assembly of simultaneous equations to be constructed to more easily determine multilayer performance. The TMM was developed specifically to predict wave propagation in in isotropic fluids and solids, through (rigid) porous materials and lightweight isotropic plates (or sheets/blankets) which perform as a limp mass. Early transfer matrix approaches assess the limp mass performance only and do not consider bending effects, which can be sufficient for lightweight plates, such as in the aerospace, automobile and marine industries.

In the TMM the principle difficulty is to determine the transfer

Abbreviations: ETICS, external thermal insulation composite system; SEA, statistical energy analysis; TMM, transfer matrix method; PIM, progressive impedance method; FTMM, finite transfer matrix method; EPS, expanded polystyrene.

* Corresponding author.
E-mail addresses: claire.churchill@tuwien.ac.at (C. Churchill), thomas.bednar@tuwien.ac.at (T. Bednar), hmuellner@tgm.ac.at (H. Müllner), maximilian.neusser@acom-research.eu (M. Neusser), simon.hinterseer@tuwien.ac.at (S. Hinterseer).

https://doi.org/10.1016/j.buildenv.2021.107807
Received 26 October 2020; Received in revised form 27 February 2021; Accepted 11 March 2021
Available online 24 March 2021

matrices with sufficient accuracy. This methodology has resulted in the development of numerous calculation methods which may be supported by a variety of measurement methods (e.g. with an impedance tube [15,16] or flow resistivity measurements [17]). The methodology also has some shortcomings; first the TMM is based on infinite plate theory, second the diffusivity of the field conditions must be correctly assessed to achieve an appropriate result, and third the structural connections, although relatively simple to implement in the PIM are more difficult to accommodate when using the TMM [18]. These disadvantages have been addressed in a number of works. In an infinite plate theory, the radiation efficiency below the critical frequency is zero. There may also be calculation problems at the critical frequency where the radiation efficiency is undefined for infinite plates. Spatial windowing was introduced to quantify the radiation efficiency below the critical frequency [19]. This is sometimes referred to as the finite transfer matrix approach (FTMM) [20]. However, there can be disagreement about the best way to apply this method to ensure goodness of fit with measured data [21]. The question of sufficient diffusivity was first addressed with the field incidence mass law which is attributed to Beranek [21]. An incident angle distribution on the surface of 0°–78° was recommended. Other distributions have since been proposed including the Gaussian based distribution [22] or other angle ranges [23]. In the case of structural connections, semi-empirical correction factors may be required. Existing methodologies to incorporate structural corrections are discussed in more detail below. Later developments of the transfer matrix method (TMM) include incorporating the effects of plate bending stiffness [15,21] and longitudinal and shear wave propagation through solids [24].

Rhazi and Atalla [20], with a particular focus on mechanical excitation, distinguish the SEA method from the TMM methods in terms of the radiation factors implemented: In SEA a frequency averaged radiation approach such as Leppington [25] may be used, whereas in the TMM a radiation impedance is preferred. The SEA method is based on power flows determined by the difference in modal energy between the component parts [26]. The component parts termed “subsystems” are coupled by means of loss factors and the modal energy is used as a temperature analogue to determine the power flows. The SEA framework has been used to determine the sound insulation of single and cavity walls [27,28]. In this paper a SEA based approach is the preferred method to determine the sum and difference between the power flow paths through a single leaf heavyweight wall, with and without the thermal insulation system, to determine the ΔR.

Wave based or semi-empirical approaches may also be based on an infinite plate approach (e.g. [18,21,23]) and use travelling wave descriptions to describe bending waves on plates and their acoustic coupling to the surrounding gases. They may also be used to combine different methodological approaches such as in the case of implementing structural connections in the TMM by means of a semi-empirical correction [18]. Rabold and Bacher [11] outline several methodologies to execute simple empirical corrections to previous calculation methods to account for a commonly observed plateau in ΔR at high frequencies (i.e. $f > f_K$ termed the “kink” frequency) due to the structural connections of the thermal insulation system. The “kink” frequency is defined as $f_K = 3.9 f_0 \sqrt{d_0 \rho_{s,3} / d \rho_{s,2}}$, where d is the distance between the walls, $d_0 = 1.0$ m is a normalising factor, $\rho_{s,2}$, $\rho_{s,3}$ are the mass per unit areas of the walls and $f_0 = 1/2\pi \sqrt{s'(1/\rho_{s,2} + 1/\rho_{s,3})}$, where s’ is the dynamic stiffness. The value of s’ is appropriate to the application; this can therefore refer to the dynamic stiffness of the elastic interlayer only, the air only, a modified value to accommodate air plus a porous material or a combination of these plus the spring stiffness of the connectors, see Eqn. (4) below. The methodologies described outline the basis for the single figure ΔR tables and calculation methods of the EN12354 ANNEX D standard.

Measurement surveys and round robins (e.g. [7–9,29]) have driven the development of empirical models. In the case of single figure sound insulation improvement, ΔR_W, given in the standard EN12354 ANNEX D, the original dataset for the empirical model appears to be a data base of about 200 sound insulation measurements upon which additional correction factors (see Fig. 1 below) were later developed [10]. More recent measurement surveys (e.g. [3,6,11,30,31]) include modern features and materials including recycled products. More unusual blockwork features such as slotted blocks (e.g. [9,10]) might also require further adjustment to the methodology used to calculate the spring stiffness of the air, s’ and hence, f_0. The acoustic prediction standard EN12354-1 ANNEX D [32] hints at some of the difficulties in deriving a generalised method for the prediction of frequency dependant sound insulation improvement (ΔR) of an additional layer of material, such as in external thermal insulation systems. Sound insulation improvement differs in the cases of airborne transmission and flanking transmission, and it may also differ in the case of a heavyweight or lightweight base wall. In all cases, it is possible to measure the frequency range 50 Hz–5000 Hz, using the methodology described in EN ISO 10140-1 ANNEX G [33]; however, the capacity to predict (or, indeed, to apply measured results to a different type of construction [34]) is less certain.

The prediction standard endeavours to provide a simple methodology to predict the single figure weighted sound insulation improvement (ΔR_W) of an additional layer, and the recognition that different system “types” will give different single figure values is already part of EN12354. Two categories are used (mineral wool, and foam) in order to incorporate the thermal insulation types available on the market (see Fig. 1) and the methodology of the standard to predict weighted sound insulation improvement is illustrated in the flowchart in Fig. 1. To account for the variety of systems, layers are classified in EN12354-1 ANNEX D [32] according to categories that include: the type of application (airborne or flanking transmission), the base wall type onto which they are installed, interior or exterior use, insulation type, whether studs, battens, or anchors are used, and the percentage of the glued area.

The weighted sound insulation improvement is determined by an empirical formula based on the spring-mass resonant frequency of the system (f_0). However, empirical regression models tend to be useful only for very specific construction categories [35]. Application of a single regression model to many different categories is unlikely to result in a useful convergence of the data on a solution. In addition, improved connection technology has shifted the resonance frequency into the low-frequency region of the building acoustics range. This has increased the relative importance of characterising the structure-borne transmission through the connections or mounting system. Systems with a similar f_0 are experimentally shown to give very different single-figure values [34] (e.g. using different materials for the weatherproof covering).

The accuracy of the calculation process is estimated by means of a standard deviation (cited as 2 dB in EN12354-1 ANNEX D [32]). However, the typology is restrictive. The variety of modern systems is such that, in practice, the identification key covers only a few limited examples. Modern systems cannot be precisely grouped by system type [1,36]; innovative materials, shapes, or forms, environmentally sustainable alternative insulation types, or recycled materials that might have different physical properties are all unaccounted for (e.g. mineral wool or foams are the only listed insulation types).

In this context, a model is required to account for sophisticated modern systems on the market. This paper explores the possibility of predicting frequency dependant sound insulation improvement of thermal insulation wall lining systems installed on the building exterior and describes methods to quantify some of the uncertainties. The work focusses on the airborne transmission of thermal insulation systems installed on heavyweight base walls; therefore, the methodology may require adaptation to accommodate lightweight base walls. In the case of the former, the transmission paths may be more easily separated from the properties of the base construction and the resulting simplified calculation makes use of this advantage. The work explores potential

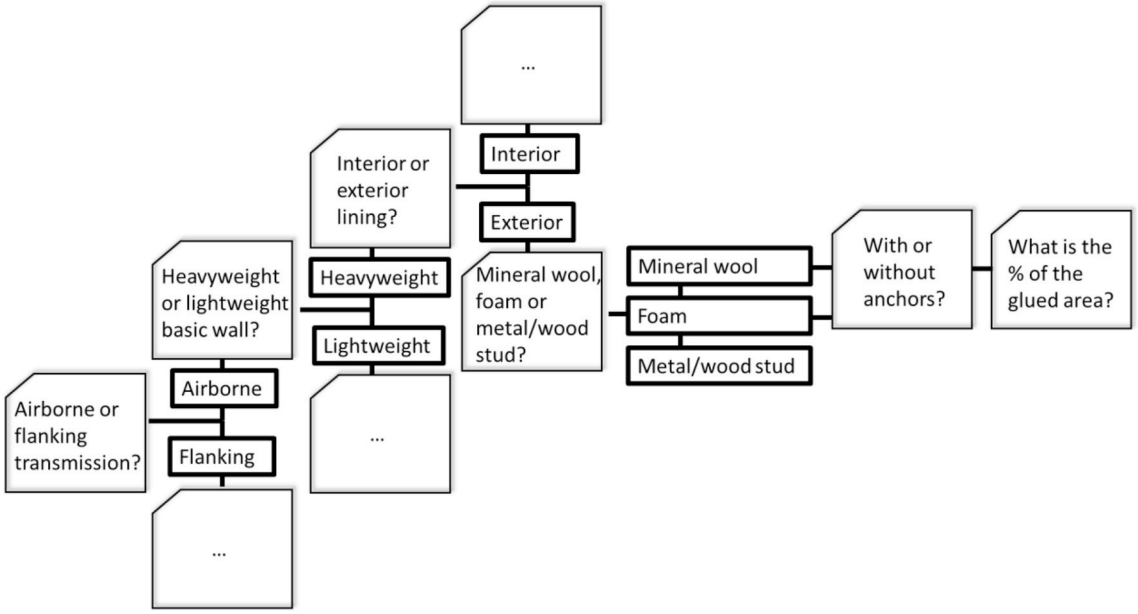

Fig. 1. Navigating the typology of the prediction process with an identification key (EN12354-1 ANNEX D [32]) for additional layers to determine the ΔR_W, weighted sound insulation improvement, of thermal insulation cladding systems installed on heavyweight exterior walls.

benefits and difficulties of introducing a methodology to calculate the sound insulation improvement of thermal cladding systems.

2. Methodology

A simple calculation procedure is required to determine the sound insulation improvement of wall cladding systems from target parameters of the construction such as spring-mass resonance (f_0) of the wall mounting system and critical frequency (f_c) of the weatherproof layer. Some basic material properties of the weatherproof layer, such as thickness and density, are also required. A previous calculation procedure [34] is revised to align the input parameters that contribute to the calculated sound insulation improvement at high and low frequencies, i.e. to give a single resonance frequency that describes both the spring-mass resonance behaviour and the structure-borne transmission through the combined thermal interlayer and wall mounting system. While the earlier calculation approach seeks to assess the influences of the elastic interlayer and the wall mounting system separately, this work seeks to combine and simplify the procedure.

The calculation procedure is compared with sound insulation improvement measurements made in an accredited Austrian laboratory in accordance with EN ISO 10140-1 ANNEX G [33]. In the subsequent sections of this paper the theory of the calculation procedure is described in section 3. The laboratory measurement procedure is briefly described in section 4. The calculation procedure was compared with the measured ΔR of four thermal insulation systems. The required input parameters for the model are discussed in section 5. Results and accuracy are discussed in sections 6 and 7. The accuracy of the procedure is assessed using three factors: (1) precision of the measurement, (2) variation of some of the basic parameters of the calculation procedure, and (3) an estimation of the standard error of the calculation. The precision is based on laboratory measurements, however, the procedure is based on the workmanship of the sample installation which is additional to the four factors (time, calibration, operator and accuracy) of intermediate precision described in the accuracy standard ISO5725-3 [37] (the specific workmanship conditions are described further in section 7.1). Measurement accuracy of the curtain wall systems was assessed using three of the aforementioned thermal insulation systems. However, to determine the measurement accuracy of the ETICS an additional fifth test sample was required. This sample consisted of 16 mm expanded polystyrene (EPS) installed using six dowels and sealed with a 5 mm weatherproof render.

Some parameters of the construction are difficult to determine accurately from the outset and are usually estimated, such as true boundary conditions of the plates, and energy transfer to the laboratory (or other flanking construction) at the plate boundaries. These factors can affect the radiation losses of the plate and the coupling losses at the plate edges respectively. The latter may increase the measured sound insulation in the laboratory, where flanking transmission is excluded from the receiving room, and this energy is then lost to the laboratory construction. The effect of these conditions is assessed in sections 7.2 and 7.3; they may in part contribute to the unexpectedly high influence of the base wall construction on the sound insulation improvement of thermal insulation systems observed in laboratory measurements [34]. Finally, the standard error of the inputs is discussed in section 7.4 and the conclusions are presented in section 8.

Known potential limitations of the calculation approach from previous work include the following factors: calculated sound insulation improvement has a low dependence on the base wall, all systems are assumed to be airtight, airborne transmission through the cavity is not modelled, and the methodologies described are likely inappropriate when the render is thin [34]. Note that in the calculation the low-frequency performance ($f < f_0$) is simply "set to zero" at frequencies below the spring-mass resonance; complicated low-frequency behaviour, although possible using the approach of [34], is not considered here. The modelling methodology may successfully predict frequency dependant sound insulation improvement, however, it was not successful in predicting single figure weighted sound insulation improvement [34].

3. Theory

3.1. The simplified expression

A simplified expression for sound insulation improvement was determined within the statistical energy analysis (SEA) framework, subscripts refer to the following subsystems (1) source room, (2) weatherproof cladding layer, (3) heavyweight base wall, (4) receiving room:

$$\Delta R = \begin{cases} 0 & (f < f_{cutoff}) \\ -10\log\left(\frac{n_2}{n_3}\frac{\eta_{21}}{\eta_{22}\eta_{31}}\eta_{23} + \frac{n_1}{n_3}\frac{\eta_{33}}{\eta_{31}\eta_{34}}\eta_{14} + \frac{n_2}{n_3}\frac{n_1}{n_3}\frac{1}{\eta_{31}\eta_{34}}\eta_{23}\eta_{14}\right) & (f \geq f_{cutoff}) \end{cases} \quad (1)$$

where η_{ij} are coupling loss factors and η_{ii} are total loss factors. When the gases in the source and receiver room are the same:

$$\Delta R = \begin{cases} 0 & (f < f_{cutoff}) \\ -10\log\left(\frac{n_2}{n_3}\frac{\sigma_2\rho_{s,3}}{\sigma_3\eta_{22}\rho_{s,2}^2}\frac{r_S}{2\pi f}Y_{eq} + \frac{n_1}{n_3}\frac{2\pi f\rho_{s,3}^2\eta_{33}}{\sigma_3^2}\frac{c_0 S_2}{V_1}|Y_{tr}|^2 \right. & \\ \left. + \frac{n_1 n_2}{n_3^2}\frac{\rho_{s,3}^2}{\sigma_3^2}\frac{c_0 S_2}{V_1}|Y_{tr}|^2\frac{r_S}{\rho_{s,2}}Y_{eq}\right) & (f \geq f_{cutoff}) \end{cases} \quad (2)$$

where σ_i is the radiation efficiencies of the panel, $\rho_{s,i}$ is the surface density of the panel, r_S is the number of structural connections, n_i is the modal density of the subsystem, c_0 is the speed of sound in air, S_i is the area of the partition V_i is the volume of the subsystem, Y_{tr} is the transfer function of the spring-mass system of the panels, f is the frequency of interest and

$$Y_{eq} = \frac{Re\{Y_3\}}{|Y_2 + Y_3 + Y_c|^2} \quad (3)$$

where Y_i is the point mobility of the panel and Y_c is the connector mobility. To further simplify this expression, in contrast to [34], which assumes different spring stiffness for the connector mobility (Y_c) and transfer function (Y_{tr}) parts of Eqn. (1), the combined connector stiffness (s') is used in both parts. This also necessitates the implicit assumption that $r_s = 1$ in Eqn. (2).

$$s' = s'_{interlayer}(1 + i\eta_{s'}) + r_S K = (s'_{interlayer} + r_S K)(1 + i\eta_{total}) \quad (4)$$

where $s'_{interlayer}$ is the interlayer stiffness, $\eta_{s'}$ is the damping of the interlayer, K is the spring stiffness of the structural connections, and η_{total} is the total damping of the combined spring system.

Expression in terms of resonance frequency (f_0)

The transfer function due to the spring-mass resonance and connector mobility can be expressed in terms of f_0 using an effective surface density of the spring-mass system:

$$\rho_{s,eff} = \frac{\rho_{s,2}\rho_{s,3}}{\rho_{s,2} + \rho_{s,3}} \quad (5)$$

and

$$f_0 = \frac{1}{2\pi}\sqrt{\frac{(s'_{interlayer} + r_S K)}{\rho_{s,eff}}} \quad (6)$$

which results in:

$$Y_c = \frac{if/\rho_{s,eff}}{2i\pi f f_0\eta_{total} + (2\pi f_0^2 - 2\pi f^2)} \quad (7)$$

The driving point mobility for bending waves on the plates is:

$$Y_i = \frac{1}{2.3\rho_i c_{L,i} h_i^2} = \frac{\pi f_{c,i}}{2.3\rho_i h_i c_0^2\sqrt{3}} = \frac{\pi f_{c,i}}{2.3\rho_{s,i} c_0^2\sqrt{3}} = 6.7x10^{-6}\frac{f_{c,i}}{\rho_{s,i}} \quad (8)$$

where $c_{L,i}$ is the longitudinal wave speed of the plate material, h_i is the thickness of the panel, and $f_{c,i}$ is the critical frequency of the plate. Therefore:

$$Y_{eq} = \frac{Re\left\{6.7x10^{-6\frac{f_{c,3}}{\rho_{s,3}}}\right\}}{\left|6.7x10^{-6\frac{f_{c,2}}{\rho_{s,2}}} + 6.7x10^{-6\frac{f_{c,3}}{\rho_{s,3}}} + Y_c\right|^2} \quad (9)$$

3.3. A semi-empirical approach

The expression in terms of the resonance frequency was simplified further to obtain a new approximate expression for ΔR without loss of generality. For plates and volumes respectively (and assuming $S_2 = S_3$, $c_0 = 343$ ms^{-1}, $\sigma_3 = 1.0$):

$$n_i = \frac{S_i\sqrt{3}}{h_i c_{L,p,i}} = \frac{\pi f_{c,i} S_i}{c_0^2} \therefore \frac{n_2}{n_3} = \frac{f_{c,2}}{f_{c,3}} \quad (10)$$

$$n_i \approx \frac{4\pi f^2 V_i}{{c_0}^3} = \frac{4\pi f^2 V_i}{{c_0}^3} \therefore \frac{n_1}{n_3} = \frac{4f^2 V_1}{f_{c,3} S_3 c_0} \quad (11)$$

$$\Delta R = \begin{cases} 0 & (f < f_{cutoff}) \\ -10\log\left(\frac{f_{c,2}}{f_{c,3}}\frac{\sigma_2\rho_{s,3}}{\eta_{22}\rho_{s,2}^2}\frac{1}{\omega}Y_{eq} + \frac{8\pi f^3}{f_{c,3}}\rho_{s,3}^2\eta_{33}|Y_{tr}|^2 \right. & \\ \left. + \frac{\rho_{s,3}}{f_{c,3}}\frac{f_{c,2}}{\rho_{s,2}}4f^2|Y_{tr}|^2\frac{\rho_{s,3}}{f_{c,3}}Y_{eq}\right) & (f \geq f_{cutoff}) \end{cases} \quad (12)$$

3.4. Heavyweight base wall

When the wall is heavyweight $\rho_{s,eff} \approx \rho_{s,2}$ typical values for $f_{c,3}$ and $\rho_{s,3}$ can be selected $f_{c,3} = 100$ Hz and $\rho_{s,3} = 500$ kgm^{-2}. The following simplifying factors are used; please note that σ_2 is a function of $f_{c,2}$ [25, 38] (see section 3.3.2):

$$A = \frac{\rho_{s,3}}{f_{c,3}}Y_{eq} = 5Y_{eq} \quad (13)$$

$$B = 4f^2|Y_{tr}|^2 \quad (14)$$

$$\Delta R = \begin{cases} 0 & (f < f_{cutoff}) \\ -10\log\left(\frac{f_{c,2}}{\rho_{s,2}^2}\frac{\sigma_2}{\eta_{22}}\frac{1}{2\pi f}A + \frac{2\pi f}{f_{c,3}}\rho_{s,3}^2\eta_{33}B + \frac{\rho_{s,3}}{f_{c,3}}\frac{f_{c,2}}{\rho_{s,2}}AB\right) & (f \geq f_{cutoff}) \end{cases} \quad (15)$$

which results in the relatively uncomplicated:

$$\Delta R = \begin{cases} 0 & (f < f_{cutoff}) \\ -10\log\left(\frac{\sigma_2(f_{c,2})f_{c,2}}{\eta_{22}\rho_{s,2}^2}\frac{1}{2\pi f}A + 5000\pi f\eta_{33}B + 5\frac{f_{c,2}}{\rho_{s,2}}AB\right) & (f \geq f_{cutoff}) \end{cases} \quad (16)$$

Set the damping of the interlayer ($\eta_{total} = 0.1$) to give a minimum reasonably close to the measured result, ~ −10 dB at f_0.

$$A = \frac{6.7x10^{-6}}{\left|6.7x10^{-6\frac{f_{c,2}}{\rho_{s,2}}} + 1.34x10^{-6} + \frac{if/\rho_{s,2}}{0.2i\pi f f_0 + (2\pi f_0^2 - 2\pi f^2)}\right|^2} \quad (17)$$

$$B = 4f^2\left|\frac{if/\rho_{s,2}}{0.2i\pi f f_0 + (2\pi f_0^2 - 2\pi f^2)}\right|^2 \quad (18)$$

In the derivation of Eqn. (16) different underlying assumptions are used to determine the high frequency performance when compared with the approach of [34]. The high frequency ΔR in the latter case is calculated using r_s, identical but statistically uncorrelated coupling

structural connections, each with spring stiffness K, which inject resonant power according to an analogue electrical circuit model [39]. The disadvantage of this approach is the model fails to predict accurate ΔR at high frequencies when there are no structural connectors. Alternatively, Eqn. (16) was derived by considering the whole façade to be a mass on a combined area spring with stiffness (s'$+r_sK$) therefore resonant power through the thermal interlayer and structural connections is correlated. This latter case is a more empirical approach, where the problem is simplified so that a single resonant frequency, f_0 is responsible for both the high frequency (resonant) and low frequency (non-resonant) performance. This has more similarity to the semi-empirical approaches of [18,40] except that a spring connector rather than a massless infinitely stiff connector is modelled. The disadvantage of this approach is (similarly to [18]) implementing a whole panel radiation efficiency results in low values for ΔR at and above f_c. This can be corrected by applying point and line radiation efficiencies in the high frequency range ($f > f_c$) required to establish the radiated power using these expressions for point and line radiation. However, in the case of spring connections (as opposed to infinitely stiff and massless connections [38,40,41]), the nearfield velocity field is more difficult to calculate. Therefore, velocity calculated from the coupled modes is used as an approximation. The nearfield radiation of the point or line sources is given by [38,40]:

$$\sigma_{B,\text{point}} = n\frac{8c_0^2}{\pi^3}\frac{1}{S}\frac{1}{f_c^2} \tag{23}$$

$$\sigma_{B,\text{line}} = n\frac{2c_0}{\pi}\frac{l}{S}\frac{1}{f_c} \tag{24}$$

where n is the number of point or line connectors respectively. If the plate has high internal losses [40], the radiation from the nearfield likely dominates the resonant transmission. The radiation from the bending modes on the plate is given by [25]:

$$\sigma_{\text{B,finite}} = \begin{cases} \dfrac{U}{2\pi\mu kS\sqrt{\mu^2-1}}\left[ln\left(\dfrac{\mu+1}{\mu-1}\right)+\dfrac{2\mu}{\mu^2-1}\right]\left[C_{BC}C_{OB}-\mu^{-8}(C_{BC}C_{OB}-1)\right] & (f<f_c) \\ \left(0.5-\dfrac{0.15L_1}{L_2}\right)\sqrt{k}\sqrt{L_1} & (f=f_c) \\ \dfrac{1}{\sqrt{1-\mu^2}} & (f>f_c) \end{cases} \tag{25}$$

where U is the plate perimeter length, $\mu = \sqrt{f_{c,2}/f}$, k is the wavenumber in air, S is the plate area, C_{BC} and C_{OB} are constants (set to values between 1 and 2) representing the boundary and baffle conditions of the plate respectively, and L_1 and L_2 are the shorter and longer dimensions of the plate respectively. The approximation $H(L_1/L_2) = 0.5 - 0.15(L_1/L_2)$ is included [25]. The reason for the coefficients C_{OB}, C_{BC} is discussed further in [39].

whereas this is not required in [34]. Alternative methods to calculate the radiation efficiency are introduced in the next section. The inclusion of an alternative radiation efficiency affects the calculation of coupling loss factors η_{21}, η_{21}, η_{43} and η_{34} which are otherwise identical to [34].

Restricting the methodology in [34] to an approach similar to Eqn. (16) and comparing the calculation of the resonant coupling loss factor η_{23} and the non-resonant coupling loss factor η_{14}. In Eqn. (16) η_{23} and η_{14} are related by Y_{tr}

$$\eta_{23} = \frac{1.34x10^{-6}}{\omega\rho_{s,2}\left|6.7x10^{-6}\frac{f_{c,2}}{\rho_{s,2}}+1.34x10^{-6}+Y_{tr}\right|^2} \tag{19}$$

$$\eta_{14} = \frac{S_2\rho_0^2c_0^3}{2\pi fV_1}|Y_{tr}|^2 \tag{20}$$

In the simplest case $Y_{tr} = \frac{if/\rho_{s,2}}{0.2if f_0+(2\pi f_0^2-2\pi f^2)}$ therefore η_{23} and η_{14} are related by f_0. In [34] η_{14} is identical to above but η_{23} only accounts for the point connectors; the stiffness of the interlayer is neglected. Therefore, in the simplest case assuming $Y_{tr} = \frac{2i\pi f}{K}$, the equivalent loss factors are

$$\eta_{23,[34]} = \frac{1.34x10^{-6}r_S}{\omega\rho_{s,2}\left|6.7x10^{-6}\frac{f_{c,2}}{\rho_{s,2}}+1.34x10^{-6}+\frac{2i\pi f}{K}\right|^2} \tag{21}$$

$$\eta_{14,[34]} = \eta_{14} \tag{22}$$

Note here that Y_c is approximated by $2i\pi f/K$ to smooth the ΔR curve at the resonance frequency of the point connection, $f_{0,\text{ point connection}}$.

3.5. Radiation efficiency

The radiation efficiency of the weatherproof lining is a function of $f_{c,2}$. This can consist of two parts: (1) the bending nearfield radiation of the point or line sources, and (2) the radiation of the plate due to the bending modes. In the first case, it is the velocity of the nearfield that is

4. Laboratory measurement of sound insulation improvement

Sound insulation improvement measurements were made in accordance with EN ISO 10140-1 ANNEX G [33]. A suitable heavyweight base wall was selected to perform the measurement. This was a single leaf 200 mm reinforced concrete wall with an estimated surface density $\rho_{s,3}$>350 kgm^{-2} and a critical frequency of about 100 Hz. The wall was without thickness resonances below 3150 Hz. The wall was installed with and without additional lining between two reverberant rooms in the 10.4 m^2 test aperture of the transmission suite. The sound insulation of the heavyweight base wall was subtracted from the sound insulation of the whole construction to obtain the ΔR in each third octave band and the ΔR_W.

5. Input parameters

Some insight into the required range of parameters can be found in the literature [2–5,7–10], or from building component manufacturers. Table 1 shows the assumed ranges of the input parameters for which the

Table 1
Input parameters to the model.

Parameter	Min	Max
f_0	20 Hz	600 Hz
$f_{c,2}$	100 Hz	5000 Hz
$\rho_{s,2}$	2.0 kgm^{-2}	40 kgm^{-2}
η_{22}	0.001	0.016

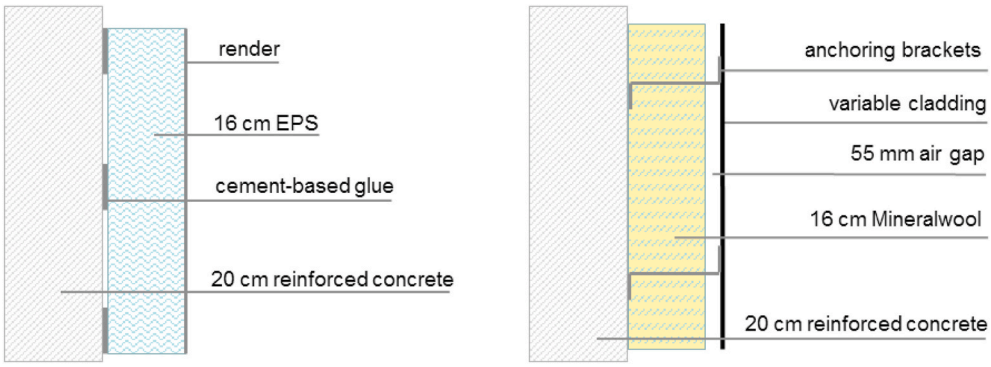

Fig. 2. Sketches of typical ETICS (without structural fixings, $r_s = 0$) and Curtain wall systems (with structural fixings, $r_s > 0$). In the diagrams shown: the mass per unit area of the reinforced concrete is $\rho_{s,3}$ or variable cladding is $\rho_{s,2}$, the spacing between the wall and covering is d, the dynamic stiffness of the EPS (or Mineralwool if required) is $s'_{interlayer}$, the spring stiffness of the anchoring brackets are K, and the mass per unit area of the render or variable cladding is $\rho_{s,2}$.

Table 2
Input data for the measured walls.

	ETICS	Curtain wall		
	Render	Fibre cement	Aluminium	Ceramic (I-section)
l x w	n/a	[a]1.60m x 0.615m	[b]1.60m x 0.734m	[c]0.9m x 0.15m
f_0	[d]275/308Hz	51.0Hz	68.4Hz	63.4Hz
s'_{air}	-	0.42MNm^{-3}	0.50MNm^{-3}	0.50MNm^{-3}
$s'_{interlayer}$	[d]41/ 52MNm^{-3}	-	-	-
r_s	12m^{-2}	1.73m^{-2}	1.73m^{-2}	1.73m^{-2}
K	0.2MNm^{-1}	0.5MNm^{-1}	0.5MNm^{-1}	0.5MNm^{-1}
$f_{c,2}$	2909Hz	2595Hz	3180Hz	[e]3120Hz
$\rho_{s,2}$	[f]15.0kgm^{-2}	[f]12.8kgm^{-2}	[f]7.5kgm^{-2}	[g]8.75kgm^{-2}
η_{22}	0.005	[h]0.005	0.001	0.007

[a] These are the dimensions of the smallest plate installed in the test facility (largest plate 2.358 m × 0.795 m).
[b] These are the dimensions of the smallest plate installed in the test facility (largest plate 2.360 m × 1.194 m).
[c] Assumed values from technical data: plate lengths (0.9–1.5 m) and plate widths (0.15–0.5 m).
[d] Note that two insulation types were installed.
[e] Note that the cut-off for the panel to behave like a repeating I-section is much higher than the frequency range of interest ($\lambda_B \gg d_R$, where λ_B is the bending wavelength and d_R is the width of the repeating I-section and in this case as an estimate $d_R \approx \lambda_B$ at 18000 Hz). Therefore, the critical frequency of the 4 mm outer panel is given. An estimated value similar to glass was used.
[f] Measured in the laboratory.
[g] An estimated value based on the geometry of the plate cross-section.
[h] An internal loss factor of up to 0.01 may be used.

calculation model might be required to deliver an appropriate ΔR.

The sound insulation improvement of four thermal insulation systems - one ETICS and three curtain wall systems (see Fig. 2) were measured in an accredited Austrian laboratory. The input data of the measured walls is summarised in Table 2. Plate lengths and widths of the smallest plates are also examined, where appropriate, to allow the first few plate bending modes to be calculated. This is used in section 6.2 to justify the appropriateness of a SEA approach. The systems are described in more detail in sections 5.1 and 5.2 below. The measured sound insulation improvement of these walls was compared with the calculation.

5.1. ETICS constructions with more than one thermal insulation type

The installation requirements of ETICS are detailed in the standards [42,43]. The ETICS specified in the research consisted of thermal insulation glued to the base wall and fixed in place using dowels that are appropriately modelled as point connections. Different numbers of dowels per unit area are possible. There are a number of situations in which two or more different types of thermally identical insulation may be installed in a building, such as the availability of building materials, budgetary considerations, etc. In instances where the acoustic properties are not identical (e.g. different dynamic stiffnesses, $s'_{interlayer,1}$ and $s'_{interlayer,2}$), it is necessary to perform the calculation for both types of insulation.

To apply the calculation procedure in such situations, it is suggested that the sound insulation improvement ΔR is calculated separately for each dynamic stiffness and a mean of the results for each interlayer calculated. Weighted averaging can then be performed according to the area coverage of each insulation type. This approach could also be used to calculate the sound insulation improvement of a statistically appropriate distribution of dynamic stiffnesses. This may alter the calculated sound insulation improvement as the dip due to the spring-mass resonance is spread over a wider frequency distribution.

In the ETICS described in Table 2, two insulation types were applied to the wall, although the area coverage of each type was not recorded. The average was applied assuming 50% of each insulation type. For this reason, two spring-mass resonance are documented in the table. In the case of both ETICS and curtain wall systems described below Eqn. (4), and Eqn. (6) were used to calculate the spring-mass resonance. In all cases the spring stiffness of the point connections was estimated; a measured value would improve the procedure. There is no generally accepted method to measure the spring stiffness of individual mounting components in ETICS or curtain wall systems and no standardised method. Such a methodology should consider factors such the performance of the connectors as they are installed with different lengths in installations with different cavity depths, compound spring effects (e.g. attachment of additional rigid or resilient studs or frameworks on which curtain walls are installed), twisting or shearing of the components, waveguide effects and any non-linear performance. A measurement method could be based on existing methodologies to measure wall ties [44] or suspended ceiling hangers [45].

5.2. Curtain wall systems

The installation requirements of curtain walls are detailed in the standards [46]. The curtain walls specified in the research were installed using a connecting framework to mount the plates. This mounting framework was also assumed to be accurately modelled using sparsely distributed point connections to represent the frame fixings. All curtain walls were installed on the same mounting framework but with slightly different air-gaps (0.24 m in the case of the aluminium laminate and 0.2 m in the case of the fibre cement and ceramic I-section), which affects the calculated spring stiffness of the air spring. As clarified in the previous section Eqn. (4), and Eqn. (6) were used for both ETICS and curtain

wall systems to calculate the spring-mass resonance; the spring stiffness of the point connections was estimated.

5.3. Curtain wall panel profiles and orthotropy

Slightly orthotropic plates in building materials are common. When the orthotropy is slight, an approximation to isotropy is often sufficient to model sound transmission. However, there are cases where the material is highly orthotropic (e.g. timber) or architectural features produce a highly orthotropic panel (e.g. strongly bound ribs or plate corrugations). Such panel profiles are common in curtain wall systems. A ceramic panel with I-section profiling was included to study the influence of orthotropy. However, the panel did not display orthotropic behaviour within the measured frequency range of interest (building acoustics range 50 Hz–5000 Hz). The sound insulation of such panels can be calculated by making separate results of sound insulation improvement in the x- and y-directions and taking the mean; to examine the influencing factors in more depth a corrugated ceramic panel is presented, as an alternative example, in section 5.3 below. The results of the moment of inertia of the cross-sectional area of the I-section only applies at high frequencies, where $\lambda_B \gg d_R$, and in this case, as an estimate $\lambda_B \approx d_R$ at 18000 Hz, where λ_B is the bending wavelength and d_R is the width of the repeating I-section.

6. Results

The calculated values are plotted against the measured results in Fig. 3 to Fig. 6. The measured results are plotted in third octave bands, as is the usual case for measurements, and the calculated results are plotted in twenty-fourth octave bands. The calculated values for an orthotropic panel are plotted in Fig. 7.

6.1. ETICS with more than one thermal insulation type

In comparing the measured results with calculated third octave bands values for the ETICS, agreement within <6.0 dB is achieved in the following third octave bands: 80–125 Hz, 200 Hz, 315 Hz, 500 Hz, 800–2500 Hz. At high frequencies, agreement is poor at and above the critical frequency of the panel, when the radiation of the whole panel is assumed. It is possible that using the radiation efficiency of the whole panel overestimates radiation at high frequencies ($f > f_c$). The calculation due to the radiating points is a closer fit to the measured results in the high frequency range (2500–5000 Hz); within <6.0 dB in all third octave bands. The trend of the measured results corroborates the calculation method and the extended dip due to the two insulation types seems to be reflected in the measured result (see Fig. 3). Inaccuracy in the resonance frequency of the mass-spring system may be because this calculation was based on some estimated values; such as of the spring stiffness of the dowels and the total damping. The calculated results may be closer to the measurement if the spring stiffness of the dowels and the total damping are also measured. The calculation method does not accurately capture the low-frequency behaviour. Peaks and troughs in the measured data at low frequencies ($f < f_0$) could be due to more complicated spring-mass behaviour of the lining or the shift of prominent modes in the room subsystems before and after the cladding was installed.

6.2. Curtain walls

A comparison of the measured results with calculated third octave band values for the three curtain wall systems revealed the following factors:

(1) For the fibre cement weatherproof layer (Fig. 4), agreement within <6.0 dB is achieved in the following third octave bands: 50–80 Hz, 125–200 Hz, 315–800 Hz, and 1250–2000 Hz. As with the ETICS systems at high frequencies, agreement is poor at and above the critical frequency of the panel when the radiation of the whole panel is assumed. In this case, the calculation due to the radiating lines of the supporting framework is a much closer fit to the measured results in the high frequency range (2500–5000 Hz); within <3.0 dB in all third octave bands.
(2) For the aluminium composite weatherproof layer (Fig. 5), agreement within <6.0 dB is achieved in the following third octave bands: 50–100 Hz and 200–2500 Hz. Agreement is poor at and above the critical frequency of the panel, when the radiation of the whole panel is assumed. The calculation due to the radiating lines of the supporting framework is a much closer fit to the measured results in the high frequency range (2500–5000 Hz); within <4.0 dB in all third octave bands. The large error bars in this case are due to fewer available measurements to calculate the

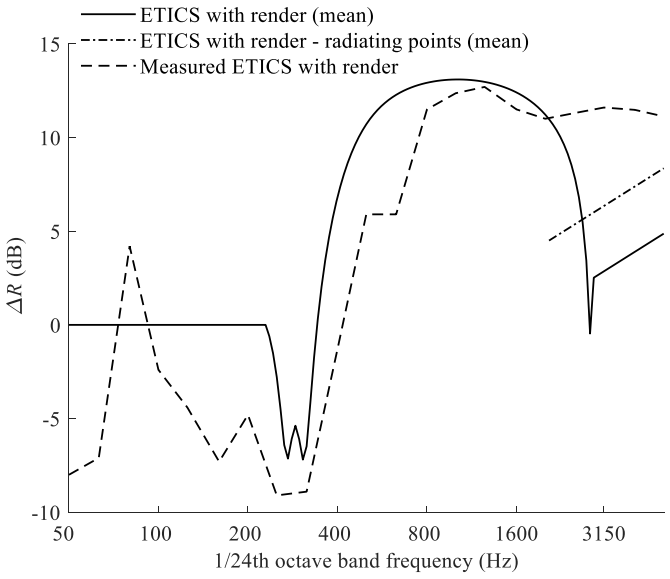

Fig. 3. ETICS installed with two insulation types (of unknown % area coverage). Calculated values are determined from f_0 = 275 and 308 Hz, f_c = 2909 Hz, ρ_{s2} = 15.0 kgm^{-2}, and η_{22} = 0.005.

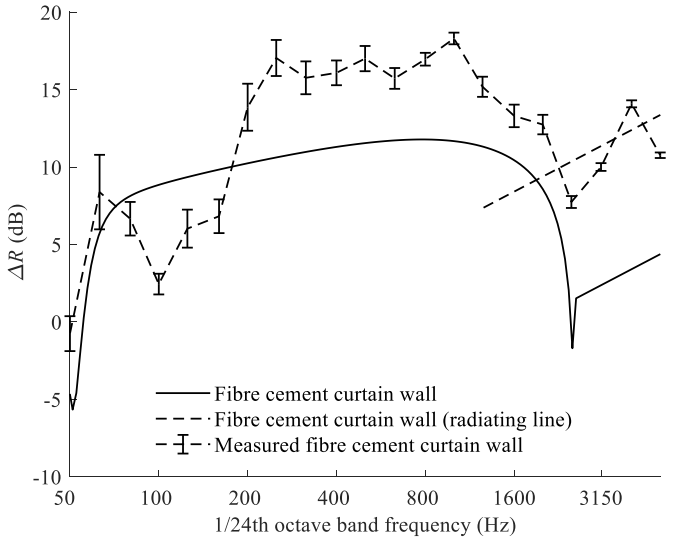

Fig. 4. Curtain wall with 4 mm fibre cement covering. Calculated values are determined from f_0 = 51.0 Hz, f_c = 2595 Hz, ρ_{s2} = 12.8 kgm^{-2}, and η_{22} = 0.005.

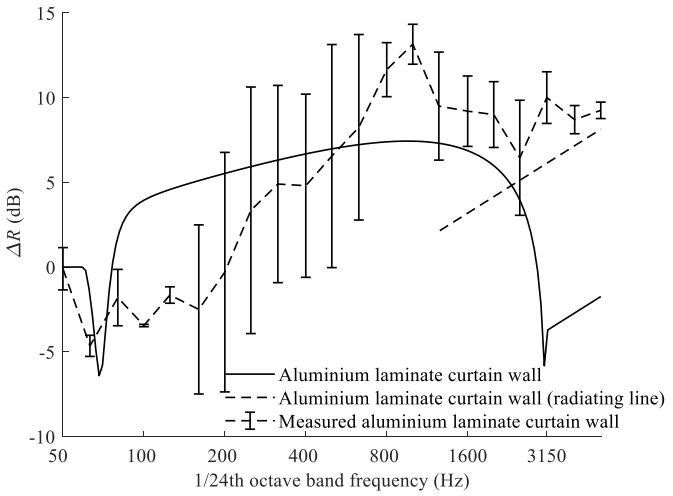

Fig. 5. Curtain wall with 8 mm aluminium laminate covering. Calculated values are determined from $f_0 = 68.4$ Hz, $f_c = 3180$ Hz, $\rho_{s2} = 7.5$ kgm^{-2}, and $\eta_{22} = 0.001$.

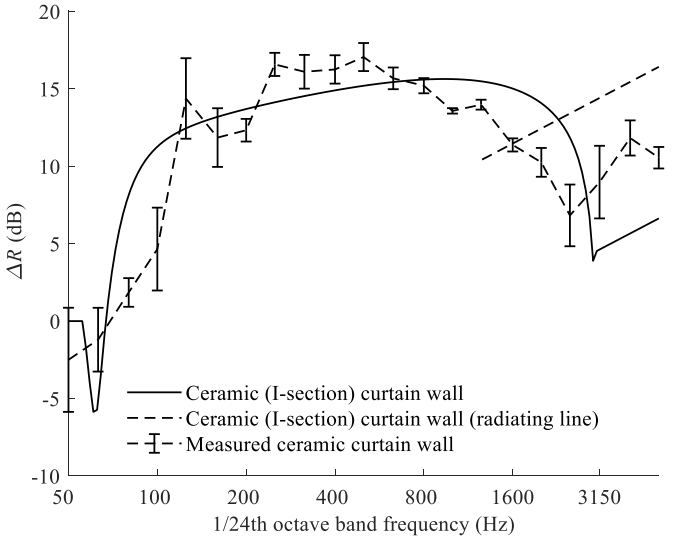

Fig. 6. Curtain wall with ceramic I-section covering. Calculated values are determined from $f_0 = 63.4$ Hz, $f_c = 3120$ Hz, $\rho_{s2} = 8.75$ kgm^{-2}, and $\eta_{22} = 0.007$.

95% confidence interval, just two measurements, in this case, compared with five and four for the other curtain walls.

(3) For the ceramic I-section weatherproof layer (Fig. 6), agreement within <6.0 dB is achieved in the following third octave bands: 50–63 Hz, and 125–4000 Hz. Good agreement is achieved at and above the critical frequency of the panel, when the radiation of the whole panel is assumed. The calculation due to the radiating lines of the supporting framework is similarly a good fit to the measured results in the high frequency range (3150–5000 Hz); within <6.0 dB in all third octave bands.

For the curtain wall systems, the trend of the measured results is not closely reflected in the calculation method, and most of the calculated results fall outside of the 95% confidence limits. The first few bending modes of the smallest plates for each weatherproof covering are shown in Table 3.

The fibre cement and aluminium composite plates support sufficient bending modes at low frequencies to assume that the distribution of bending modes within the building acoustics range (50–5000 Hz) is

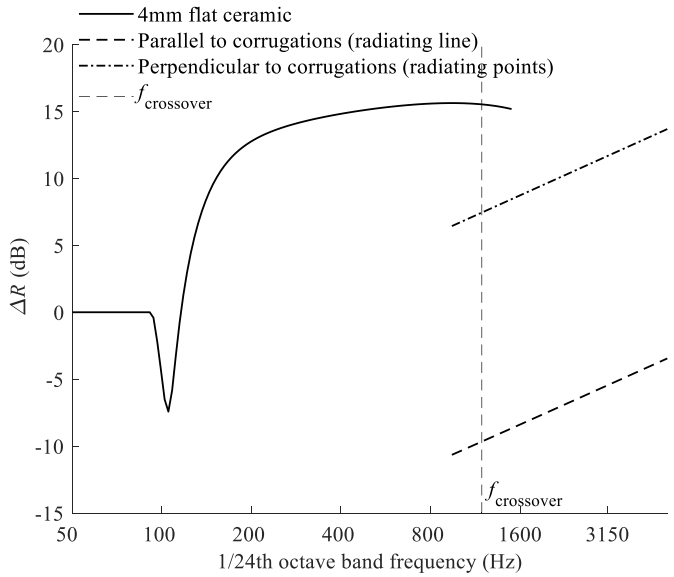

Fig. 7. Curtain wall with corrugated covering. Calculated values are determined from $f_0 = 104$ Hz, $f_c = 3120$ Hz, $\rho_{s2} = 3.2$ kgm^{-2}, and $\eta_{22} = 0.007$.

Table 3
Bending modes of the smallest plates in each curtain wall system.

	Fibre cement	Aluminium	Flat ceramic
l x w	1.60 m × 0.615 m	1.60 m × 0.734 m	0.9 m × 0.15 m
$f_{1,1}$	34.4 Hz	20.8 Hz	430 Hz
$f_{1,2}$	124.3 Hz	72.3 Hz	1688 Hz
$f_{2,1}$	47.7 Hz	31.6 Hz	466 Hz

sufficient to apply a SEA approach. However, the ceramic plates are smaller, and (if a 4 mm thick flat plate is assumed) support no bending modes below 430 Hz. Therefore, an alternative model may be required at low frequencies, and a calculation model that accounts for a sparse distribution of prominent modes rather than a statistical distribution may be more appropriate in the mid-frequency range. Other limitations, which may affect all systems, include the assumption of airtightness in combination with unaccounted airborne transmission into and out of the cavity. Although the mechanism by which greater than expected sound insulation is achieved is uncertain, it is possible that less airtightness may mean the air-spring stiffness of these systems is no longer important. Some key input parameters were estimated (e.g. spring stiffness of the fastenings, internal loss factor, and critical frequency of the weatherproof layer) and should be verified in further work. It may also be beneficial in these cases to measure the spring-mass behaviour of these systems to rule out other causes. However, this is less likely to be the source of the discrepancy between measured and calculated results. In these systems, the low-frequency behaviour is pushed to the low end or shifted below the building acoustics range (50–5000 Hz).

6.3. Curtain wall panel profiles and orthotropy

Orthotropic panels are an interesting case; orthotropy is common in materials used for building applications. However, the methodology by which orthotropic properties should be included to calculate acoustic metrics, and the degree to which this influences the result is often unclear. Unfortunately, the ceramic panel with I-profiling, measured in the study, did not prove to be orthotropic within the building acoustics range (50 Hz–5000 Hz). Therefore, a comparison of the calculation of ΔR with measured results was not possible. However, the calculated results for an alternative typical orthotropic panel profile, in this case a corrugated panel, is shown in Fig. 7. Some of the factors to predict the sound insulation improvement of a typical orthotropic panel are

discussed in detail below.

The model for a flat ceramic panel is used for most of the frequency range. Although the panel shape works to increase the radiating area, which may affect the radiation of the panel, it is assumed this is a close enough approximation. The connector model must be determined, and, in this instance, a point connection approach was used, reflecting the number of point fixings to hold the supporting framework to the base wall. Assuming substitution to a line model when the connection spacing is half the bending wavelength [41] and a point connection spacing of 0.8 m, substitution to a line model would only be necessary below $f_{line}<16$ Hz.

The appropriate radiation must be determined for the corrugated plate. To correctly predict the radiation from the weatherproof covering at high frequencies ($f > f_{crossover}$), a number of observations are required. The structural fastenings between the supporting framework and the weatherproof panel, assumed in this case to be studs, can be oriented in the direction parallel or perpendicular to the corrugations, which may require different modelling assumptions. If the studs are oriented in the direction perpendicular to the corrugations, a point radiation model may be more appropriate due to the contact with the panel (see Fig. 8). If the studs are oriented in the direction parallel to the corrugations a point or line model may be possible. Finally, please note that the panel has a high bending stiffness in the direction parallel to the corrugations. In this case, the consequence is that the plate supports no modes parallel to the corrugations for most of the building acoustics range ($f < 4000$ Hz).

Addressing some of these concerns can lead to wide variations in modelled sound insulation improvement. In the example presented in Fig. 7, it may be most appropriate to select the radiating point data using the bending stiffness perpendicular to the corrugations at high frequencies, particularly since the plate supports no bending modes parallel to the corrugations. However, without guidance based on measured data, it can be difficult to select and apply the most appropriate method. Further work on the significance and impact of orthotropic behaviour on modern curtain wall systems in airtight (and non-airtight) installations is therefore required.

7. Error estimation

7.1. Precision

The precision due to two different workmanship factors was assessed (quoted as 95% confidence limits i.e. $1.96s_{I(W)}$); these were the method

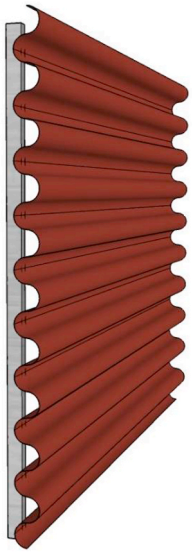

Fig. 8. Corrugated covering with supporting stud-orientation perpendicular to the corrugations.

Table 4
Precision due to workmanship 95% confidence limits for ETICS.

f (Hz)	50	63	80	100	125	160	200	250	315	400	500	630	800	1000	1250	1600	2000	2500	3150	4000	5000
ETICS (dB)	5.62	4.87	0.15	0.21	0.15	0.15	0.14	0.08	0.04	0.07	0.10	0.17	0.29	0.56	0.49	0.10	0.13	0.16	0.31	0.58	0.48

of installation of the dowels and the airtightness of the sample. The influence of the dowel installation method was relevant for the ETICS [47]. The motivation for the test procedure was to ensure that different numbers of dowels could be retrospectively fitted to a test sample to ensure efficient testing of many similar samples. The ETICS test sample was 16 mm expanded polystyrene (EPS) installed using six dowels and sealed with a 5 mm weatherproof render. The precision measure is quoted as an estimate of precision due to workmanship for ETICS. Five cases were tested, where the dowels were installed using slightly different methods. These included the dowel installed in the usual manner, the dowel installed through an opening drilled in the plaster using a hole saw (unsealed), and the dowel installed as in the latter example but sealed with render (when the render is green and when it is fully set). The results are shown in Table 4. Despite the aforementioned variations in the sample, the measurement is found to be highly repeatable. Confidence limits of less than <0.6 dB are observed for all but the lowest frequencies (50 Hz and 63 Hz).

Precision due to workmanship of the fibre cement, aluminium laminate and ceramic curtain wall systems was also assessed in the laboratory. Five, four and two measurements were made on each system respectively, using measures such as taping the seams to vary the airtightness in the range from fully open to fully closed, with an intermediate airtightness included in the cases of the fibre cement and aluminium laminate, where only joints between the positioned plates were sealed. The confidence limits are shown in Table 5. The precision measure is quoted as an estimate of precision due to workmanship for curtain wall systems. The greatest variation is seen for the aluminium laminate in the mid-frequency range (200 Hz–400 Hz and 630 Hz–800 Hz) where 95% confidence limits >5 dB are observed. This might be due to the effect of airtightness in combination with airborne transmission into and out of the cavity (briefly discussed in section 6.2). Less airtightness may mean the air-spring stiffness of these systems is no longer important, with the energy transfer paths via the connectors and cavity increasing in relative importance. The exact mechanisms are, at this stage, uncertain.

7.2. Uncertainty due to the internal and edge loss factor of the heavyweight base wall

The density and critical frequency of the heavyweight base wall can be shown to have relatively little influence on sound insulation improvement ΔR, certainly when f_{c3}<100Hz [34]. The internal and edge losses of the heavyweight wall may also be influential, and their relative importance is assessed below. The internal loss factor of the heavyweight base wall was assumed to vary between $\eta_{33} = 0.005$ (typical value for concrete cast in situ) and $\eta_{33} = 0.0125$ (typical value for concrete blocks connected with mortar) [39]. The coupling loss factors at the edges of the plate are added to the internal loss factor of the heavyweight base wall, and an empirical factor X can be used as an estimate [39]:

$$\eta_{ii} = \eta_{i,internal} + \frac{X}{\sqrt{f}} \tag{26}$$

where f is the frequency band of interest. In a previous study, the following values were used: $X = 0.8$ for the concrete heavyweight walls and $X = 0.3$ for the brick walls [34]. This provides an estimation although it would be better to measure or calculate actual coupling losses. The effect of varying X and η_{33} is shown in Table 6.

Please note that the solely "resonant" sound reduction index of the base wall is proportional to the internal loss factor. For a heavyweight wall this is proportional to the measured transmission coefficient above the critical frequency of the wall (i.e. for most of the building acoustics range). For a typical heavyweight wall the critical frequency is low; in section 3.3, $f_{c,3} = 100$ Hz is assumed. This means radiation efficiency does not vary across the building acoustics range; the radiation

Table 5
Precision due to workmanship 95% confidence limits for the three curtain wall systems.

f (Hz)	50	63	80	100	125	160	200	250	315	400	500	630	800	1000	1250	1600	2000	2500	3150	4000	5000
Fibre Cement (dB)	1.13	2.41	1.08	0.67	1.23	1.09	1.52	1.16	1.06	0.80	1.13	0.81	0.67	0.41	0.38	0.65	0.73	0.63	0.39	0.25	0.23
Aluminium (dB)	1.25	0.62	1.66	0.07	0.49	4.99	7.07	7.28	5.82	5.41	1.25	6.58	5.47	1.59	1.18	3.19	2.08	1.94	3.40	1.52	0.83
Ceramic (dB)	3.36	2.06	0.93	2.68	2.60	1.89	0.73	0.75	1.09	0.92	3.36	0.90	0.70	0.49	0.17	0.32	0.42	0.93	1.99	2.34	1.14

Table 6
Difference between maximum ($X = 0.3$, $\eta_{33} = 0.005$) and minimum ($X = 1.0$, $\eta_{33} = 0.0125$) values for sound insulation improvement ΔR due to different edge and internal loses of the heavyweight base wall.

f / f_0	1.0	1.3	1.6	2.0	2.6	3.2	4.1	5.2	6.5	8.1	10.2
f / f_{c2}	0.1	0.1	0.2	0.2	0.3	0.3	0.4	0.6	0.7	0.9	1.1
ETICS (dB)	4.9	3.7	2.0	0.9	0.4	0.2	0.1	0.0	0.0	0.0	0.0

efficiency (σ_3) is assumed to be one at all frequencies. Therefore, the measured transmission coefficient (τ_{resonant}) of the heavyweight wall may be, in some circumstances, used as a proxy for a loss factor which includes edge losses [35]:

$$\frac{1}{\tau_{\text{resonant}}} \propto \eta_{ii} \tag{27}$$

$$R_{\text{resonant}} \propto 10log(\eta_{ii}) \tag{28}$$

The maximum impact of internal loss factor and plate edge losses combined is ±2.4 at the spring-mass resonance. This is not of the appropriate magnitude or frequency range to account for measured differences on different types of base wall, which can be up to ±4.4 dB for ETICS systems at high frequencies [34]; an additional influencing factor must be present.

Efforts to determine the plate loss factor by measurement that included edge coupling were unsuccessful. As the plate edge conditions changed, the plate loss factor measurements did not alter significantly. Possible reasons for this include limitations of the available measurement equipment as T_{15} only could be measured to determine the loss factor, whereas T_5 is recommended for structural reverberation time measurements [48]. The facility to record and examine decay curves to make any appropriate adjustments manually was also not included.

7.3. Uncertainty due to the boundary and baffle conditions of the weatherproof layer

The weatherproof layer is a lightweight material with the critical frequency in the high-frequency range. This means altering the boundary and baffle conditions affects the calculation of radiation efficiency according to the factor $[C_{BC}C_{OB} - \mu^{-8}(C_{BC}C_{OB} - 1)]$ in Eqn. (25) for much of the building acoustics frequency range. The factor varies between one and four according to the combination of boundary and baffle conditions. Additionally, the value obtained using the radiation efficiency calculation may or may not be capped at one as set out in [39] for frequencies at and above f_c. The effects of these conditions are presented in Table 7.

The maximum effect on the sound insulation improvement due to different boundary conditions of the weatherproof layer is ±1.75 dB. This could contribute to measured differences when the ETICS is installed on alternative base walls: as the base wall type is altered, the boundary and baffle conditions of the weatherproof layer can change too. This is highly likely in a laboratory or field situation where different base wall types are located in different facilities or architectural designs. However, measured differences on different types of base wall can be up to ±4.4 dB for ETICS systems, indicating there must be some additional influencing factor. These factors are difficult to determine accurately and are usually estimated. It is therefore more appropriate to assume that boundary and baffle conditions contribute to an accuracy limit of the calculation procedure rather than aiming to accurately determine such conditions in every individual case.

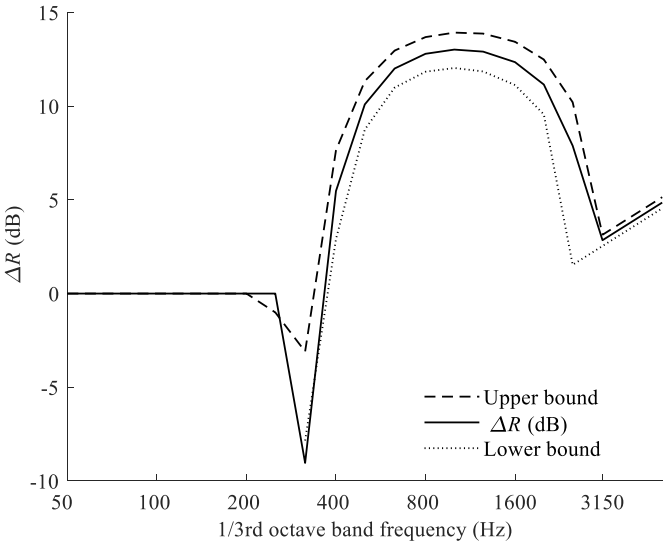

Fig. 9. Standard error due to the accuracy of the inputs: $f_0 = 310 \pm 20$ Hz, $f_c = 2900 \pm 200$ Hz, $\rho_{s2} = 15$ kgm^{-2}, $\eta_{22} = \eta_{33} = 0.005$, h = 0.01 m.

7.4. Standard error of the inputs

An estimate of the standard error due to the inputs was made based on the empirical equation Eqn. (16), using the following input values: $f_0 = 310 \pm 20$ Hz, $f_c = 2900 \pm 200$ Hz, $\rho_{s2} = 15$ kgm^{-2}, $\eta_{22} = \eta_{33} = 0.005$, h = 0.01 m. The upper and lower bounds in this case are presented in Fig. 9. This gives an impression of the effects of material measurement errors on the calculated result. The mean differences across the frequency range (250–5000 Hz) are due to the stated measurement errors ±1.3 dB. The formula for the standard error could be derived based on Eqn. (16).

8. Conclusion

For the ETICS, agreement within <6.0 dB is achieved across much of the frequency range. More than one insulation type is used in the ETICS system, and this aspect is included in the model by means of an averaging process. The trend of the extended dip due to the spring-mass action of the panel with thermal insulation of two different dynamic stiffnesses, s'$_{\text{interlayer},1}$ and s'$_{\text{interlayer},2}$ is corroborated. The assumption of radiating points gave better agreement with the measured sound insulation improvement than the assumption of a fully radiating panel at high frequencies ($f \geq 2500$ Hz). The case for using this methodology on curtain wall systems is adequate, although less convincing. For the

Table 7
The difference between the maximum ($C_{OB} = 2.0$, $C_{BC} = 2.0$) and minimum ($C_{OB} = 1.0$, $C_{BC} = 1.0$) values for sound insulation improvement ΔR due to different boundary, baffle, and calculation conditions is used to calculate the radiation efficiency of the weatherproof layer.

f / f_0	1.0	1.3	1.6	2.0	2.6	3.2	4.1	5.2	6.5	8.1	10.2	13.0	16.2
f / f_{c2}	0.1	0.1	0.2	0.2	0.3	0.3	0.4	0.6	0.7	0.9	1.1	1.4	1.7
ETICS (dB)	0.0	1.0	2.1	2.6	2.8	2.9	2.9	2.8	2.6	1.9	3.5	1.4	0.9

curtain wall systems, the simple model was able to predict sound insulation improvement of ΔR within <6.0 dB with varying degrees of success. However, the trend of calculated results is mostly outside of the 95% confidence limits of the measured results. This could be due to the lack of airtightness of all curtain wall systems: less airtightness may reduce the importance of the air-spring stiffness and increase the importance of transmission due to radiation into and out of the cavity. Additionally, the ceramic plates support no bending modes below 430 Hz, and alternative models may be more appropriate. A model which incorporates airborne transmission through the cavity may also be beneficial. For two of the three curtain wall systems, the assumption of a radiating line gave better agreement with the measured sound insulation improvement than the assumption of a fully radiating panel at high frequencies ($f \geq 2500$ Hz). The spring stiffness of the structural connections and spring behaviour of the mounting systems were estimated and should be verified in further work.

Orthotropic panels increase the complexity of the calculation procedure and different modelling approaches may lead to wide variations in modelled sound insulation improvement. The significance and impact of orthotropic behaviour in airtight (and non-airtight) installations is also unclear. Further work is required to determine high-frequency behaviour ($f > f_{\text{crossover}}$) of such systems and ensure the input parameters are not oversimplified. The decision to use a point or line radiation at high frequencies may depend on the precise geometry of the panel. Flaws in the calculation procedure should be investigated in further detail and a wider range of systems should be compared and contrasted.

Estimates of the precision for all systems are tabulated in Tables 4 and 5. Modelling variations due to different edge and internal loses of the heavyweight base wall are tabulated in Table 6 and the modelling variations due to different boundary, baffle, and calculation conditions, used to calculate the radiation efficiency in Table 7. The latter is the most likely cause of measured differences when the ETICS is installed on alternative base walls. These factors all contribute to the limit of achievable accuracy of the calculation procedure.

Declaration of competing interest

The authors declare the following financial interests/personal relationships which may be considered as potential competing interests: MN was employed or contracted by the following private companies and consultancies: ACOM Research, Kienegg 27, 2813 Thomasberg (https://www.acom-research.eu/) and Unternehmensberatung Rudolf Exel, A-7423 Grafenschachen 343 (http://beratung.exel.at). These companies provide management and consultancy in topics including noise, sound insulation and room acoustics. These affiliations are not thought to have significantly influenced paper content or outcomes. The remaining authors work for academic institutes.

Acknowledgements

The work carried out in this project was supported jointly by the FFG (Österreichische Forschungsförderungsgesellschaft) (60% funding) [Projektnummer: 864983], and commercial project partners (40% funding). We gratefully acknowledge Michaela Smertnig and Johannes Zeilinger from Ecoplus, Niederösterreich-Ring 2, Haus A, 3100 St. Pölten for project management and guiding communication with the commercial project partners. The authors acknowledge TU Wien Bibliothek for financial support through its Open Access Funding Programme.

References

[1] P. Liška, B. Nečasová, B. Kovářová, M. Novotný, Revitalization of Lightweight Cladding of Buildings and its Impact on Environment, Prague, in World Multidisciplinary Earth Sciences Symposium, 2017.
[2] C. Guigou-Carter, R. Foret, M. Villot, J.-B. Chéné, Effect of thermal renovation on acoustic performance of buildings, in Euronoise, Edinburgh, Scotland, 2009.
[3] J. Nurzynski, The Effect of Additional Thermal Lining on the Acoustic Performance of a Wall, in *Euronoise*, Paris, France, 2008.
[4] L. Parati, B.P. Farbood, M. Borghi, May retrofit also include acoustics aspects? Energy Procedia 78 (2015) pp158–163.
[5] A. Magrini, F. Scamoni, C. Scrosat, Integrated Acoustic and Thermohygrometric Performances of Building Walls, for More Efficient Refurbishment Strategies: First Evaluations, in ICSV21, Beijing, China, 2014.
[6] K. Miskinis, V. Dikavicius, A. Buska, Acoustical and thermal properrties of building envelope with ETICS, in: in ICSV23, Athens, Greece, 2016.
[7] T.D. Northwood, D.W. Monk, Sound Transmission Loss of Masonry Walls: Twelve Inch Lightweight Concrete Blocks with Various Surface Finishes, Canada, NRC, Ottawa, 1974.
[8] A.C.C. Warnock, Sound transmission through concrete blocks with attached drywall, J. Acoust. Soc. Am. 90 (3) (1991) 1454–1463.
[9] A.C.C. Warnock, D.W. Monk, Sound Transmission Loss of Masonry Walls - Tests on 90 140, 190, 240 and 290mm Concrete Block Walls with Various Surface Finishes, Canada, NRC, Ottawa, 1984.
[10] L. Weber, S. Müller, Schallschutz bei Wärmedämm-Verbundsystemen, Frauhofer IRB, Stuttgart, 2015.
[11] A. Rabold, S. Bacher, Wärmedämmverbundsysteme und Außendämmungen aus nachwachsenden Rohstoffen zum Einsatz in der Altbausanierung – Prognose und Optimierung der schalltechnischen Eigenschaften, Frauhofer IRB, Stuttgart, 2014.
[12] A. Alonso, J. Patricio, S. Rafael, R. Escandón, Acoustical Retrofit of Existing Residential Buildings: Requirements and Recommendations for Sound Insulation between Dwellings in Europe and Other Countries Worldwide, 174, Building and Environment, 2020.
[13] M. Fringuellino, C. Guglielmone, Progressive impedance method for the classical analysis of acoustic transmission loss in multilayered walls, Appl. Acoust. 59 (2000) 275–285.
[14] L.L. Beranek, G.A. Work, Sound transmission through multiple structures containing flexible blankets, J. Acoust. Soc. Am. 21 (4) (1949) 419–428.
[15] C.M. Lee, Y. Xu, A modified transfer matrix method for prediction of transmission loss of multilayer acoustic materials, J. Sound Vib. 326 (2009) 290–301.
[16] B. Song, J.S. Bolton, A transfer-matrix approach for estimating the characteristic impedance and wave numbers of limp and rigid porous materials, J. Acoust. Soc. Am. 107 (2000) 1131–1152.
[17] B. Brouard, D. Lafarge, J.F. Allard, A general method of modelling sound propagation in layered media, J. Sound Vib. 183 (1) (1995) 129–142.
[18] T.E. Vigran, Sound transmission in multilayered structures - introducing finite structural connections in the transfer matrix method, Appl. Acoust. 71 (2010) 39–44.
[19] M. Villot, C. Guigou, L. Gagliardini, Predicting the acoustical radiation of finite size multi-layered structures, J. Sound Vib. 245 (3) (2001) 433–455.
[20] D. Rhazi, N. Atalla, Transfer matrix modeling of the vibroacoustic response of multi-materials structures under mechanical excitation, J. Sound Vib. 329 (2010) 2532–2546.
[21] A. Pellicier, N. Trompette, A review of analytical methods, based on the wave approach, to compute partitions transmission loss, Appl. Acoust. 68 (2007) 1192–1212.
[22] H.-J. Kang, J.-G. Ih, J.-S. Kim, H.-S. Kim, Prediction of sound transmission loss through multilayered panels by using Gaussian distribution of directional incident energy, J. Acoust. Soc. Am. 107 (2000) 1413.
[23] J.L. Davy, Predicting the sound insulation of walls, Build. Acoust. 16 (1) (2009) 1–20.
[24] M.L. Munjal, Response of a multilayered infinite plate to an oblique plane wave by means of transfer matrices, J. Sound Vib. 162 (2) (1993) 333–343.
[25] F.G. Leppington, E.G. Broadbent, K.H. Heron, The acoustic radiation efficiency of rectangular panels, Proc. Roy. Soc. Lond. A 382 (1982) 245–271.
[26] R.H. Lyon, Part I: Basic Theory. *Statistical Energy Analysis of Dynamical Systems*, Massachusetts Institute of Technology, 1975, pp. 3–169.
[27] M.J. Crocker, A.J. Price, Sound transmission using statistical energy analysis, J. Sound Vib. 9 (3) (1969) 469–486.
[28] M.J. Crocker, A.J. Price, Sound transmission through double panels using statistical energy analysis, J. Acoust. Soc. Am. 47 (3) (1970) 683–693.
[29] J. Lang, A round robin on sound insulation in buildings, Appl. Acoust. 52 (3/4) (1997) 225–238.
[30] J. Kümmel, Effects of thermal insulation on the airborne sound insulation, Special Issue: ICAAC - 6th International Conference on Autoclaved Aerated Concrete 2 (4) (2018) 89–95.
[31] L. Nowotny, J. Nurzynski, The influence of insulating layers on the acoustic performance of lightweight frame floors intended for use in residential buildings, Energies 13 (2020) 1–15.
[32] ISO12354-1 Building Acoustics - Estimation of Acoustic Performance of Buildings from the Performance of Elements Part 1: Airborne Sound Insulation between Rooms, International Organization for Standardization, 2017.
[33] ISO10140-1 Acoustics — Laboratory Measurement of Sound Insulation of Building Elements, International Organization for Standardization, 2016.
[34] C. Churchill, T. Bednar, H. Müllner, M. Neusser, S. Hinterseer, A parametric study of the acoustic properties of thermal cladding systems, Appl. Acoust. 173 (2021), 107656.
[35] M. Neusser, H. Müllner, C. Churchill, Schallschutz WDVS - Modell und Prognose Mechanismen der Luftschallübertragung durch Außenwände mit Wärmedämmverbundsystem und dessen Prognose, in 7. BauphysikerInnen-Treffen, Veranstaltungszentrum MA39 Prüf-Inspektions- und Zertifizierungsstelle der Stadt Wien, 2020.

[36] U.Y.A. Tettey, L. Gustavsson, Primary energy and CO_2 emissions implications of different insulation, cladding and frame materials for residential buildings, in Emerging Concepts for Sustainable Built Environment (2019).
[37] ISO5725-3 Accuracy (trueness and precision of measurement methods and results) - Part 3: intermediate measures of the precision of a standard measurement method, International Organization for Standardization (1994).
[38] T.E. Vigran, Building Acoustics, Taylor & Francis, 2008.
[39] C. Hopkins, Sound Insulation, Elsevier, 2007.
[40] L. Cremer, M. Heckl, B.A.T. Petersson, Structure-Borne Sound, Springer, Germany, 2005.
[41] R.J.M. Craik, R.S. Smith, Sound transmission through double leaf lightweight partitions. Part I: airborne sound, Appl. Acoust. 61 (2000) 223–245.
[42] EN13499 Thermal Insulation Products for Buildings - External Thermal Insulation Composite Systems (ETICS) Based on Expanded Polystyrene - Specification, European Committee for Standardization, 2003.
[43] EN13500 Thermal Insulation Products for Buildings. External Thermal Insulation Composite Systems (ETICS) Based on Mineral Wool. Specification, European Committee for Standardization, 2003.
[44] R.J.M. Craik, R. Wilson, Sound transmission through masonry cavity walls, J. Sound Vib. 179 (1) (1995) 79–96.
[45] J. Brunskog, P. Hammer, Measurement of the acoustic properties of resilient statically tensile loading devices in lightweight structures, Build. Acoust. 9 (2) (2002) 99–137.
[46] EN13830 Curtain walling, Product Standard, European Committee for Standardization, 2020, 2015+A1.
[47] M. Neusser, N.B. Roozen, H. Müllner, S. Hinterseer. Messung des Einflusses von Dübeln zur Befestigung von Wärmedämmverbundsystemen auf das Luftschalldämmmaß von Außenwänden in Massivbauweise, in DAGA, Rostock, Germany, 2019.
[48] M. Robinson, C. Hopkins, On the evaluation of decay curves to determine structural reverberation times for building elements, Acta Acustica united Acustica 99 (2013) 226–244.